communications physics

Article

A Nature Portfolio journal

https://doi.org/10.1038/s42005-025-02310-y

Memory loss is contagious in open quantum systems

Anael Ben-Asher [1,2] ✉, Antonio I. Fernández-Domínguez [1,2] ✉ & Johannes Feist [1,2] ✉

Markovian (memoryless) system-bath interactions play a fundamental role across physics, chemistry, and biological systems. Typically, such memoryless behavior arises from the bath's properties. Here, we reveal a distinct mechanism: when a system interacts with both a Markovian and a non-Markovian bath, losses induced by the former suppress memory effects from the latter, making the interaction appear more Markovian. This effect leads to a direct interplay between independent baths, where Markovianity becomes "contagious," transferring between them via their common system. To describe this phenomenon, we introduce a Bloch-Redfield-inspired approach that accurately captures how a lossy system, governed by a Lindblad master equation, interacts with a non-Markovian bath. Beyond offering new insights into dissipative dynamics, this framework provides a computationally efficient alternative for modeling complex system-bath interactions across a broad range of scientific disciplines.

No physical system is ever fully isolated from its environment, and the possibility of exchanging energy or particles with the baths/reservoirs in the environment induces dissipation. This is a fundamental aspect of open quantum systems[1,2], ubiquitous in nature and technology. System-bath interactions are typically classified as either Markovian (memoryless) or non-Markovian. Markovianity, which refers to the evolution of a system that depends only on its present state, holds great importance not only for characterizing many processes but also as an efficient approximation that reduces conceptual and computational complexity[1–5]. In open quantum systems, the bath autocorrelation function $C(t)$ describes the memory the bath retains at time $\tau + t > \tau$ of its interaction with the system at time τ[1,2]. Therefore, a bath is considered Markovian when $C(t)$ decays to zero faster than any other timescale of the problem, a property determined by the internal structure and dynamics of the bath.

When a system interacts simultaneously with Markovian and non-Markovian baths, its dynamics are affected by the interplay between the two. For example, it was shown that the non-Markovian bath governs the dynamics at early times, while the Markovian bath dominates at later times[6]. More generally, when two independent baths interact with the system through coupling operators that do not commute with each other or with the system Hamiltonian, they cannot be described by a single effective bath whose effect is merely the sum of the individual effects of both of them[7–10]. Accounting for their nonadditive effect usually requires computationally demanding approaches such as tensor network methods[9] or approximate methods such as the reaction coordinate framework[10,11] or the polaron transformation[12].

In this article, we demonstrate that the interplay between a Markovian and a non-Markovian bath, both coupled to the same system (as sketched in Fig. 1), can induce a distinct type of memoryless interaction. Specifically, dissipation from the Markovian bath causes the system to lose memory of the non-Markovian bath faster than predicted by the bath's properties alone, effectively rendering the originally non-Markovian interaction memoryless. This implies that, in some sense, Markovianity is "contagious" and can be transferred from one bath to another through the system with which they both interact. We capture this effect using a master equation derived within the interaction picture of the effective non-Hermitian (NH) Hamiltonian[13], which describes the coherent part of the system dynamics due to the memoryless bath. This framework accounts for the decay of coherence in the system over time, causing the system's eigenstates to "forget" the correlation function of the originally non-Markovian bath. As a result, the system no longer samples the bath with unlimited frequency resolution, averaging out fine details in a way that gives rise to an emergent Markovian interaction. Our memoryless master equation thus incorporates both baths and naturally accounts for their nonadditivity, providing a computationally efficient alternative to existing methods, with broad applicability in quantum mechanics, including optics[14], acoustics[15], quantum thermodynamics[16–18], and chemistry[19–21].

Results and Discussion

In this section, we first introduce the Bloch-Redfield for lossy systems (BR LS) approach, which yields a memoryless master equation that captures the effects of both Markovian and non-Markovian baths, including their

[1]Departamento de Física Teórica de la Materia Condensada, Universidad Autónoma de Madrid, Madrid, Spain. [2]Condensed Matter Physics Center (IFIMAC), Universidad Autónoma de Madrid, Madrid, Spain. ✉e-mail: anaelba0@gmail.com; a.fernandez-dominguez@uam.es; johannes.feist@uam.es

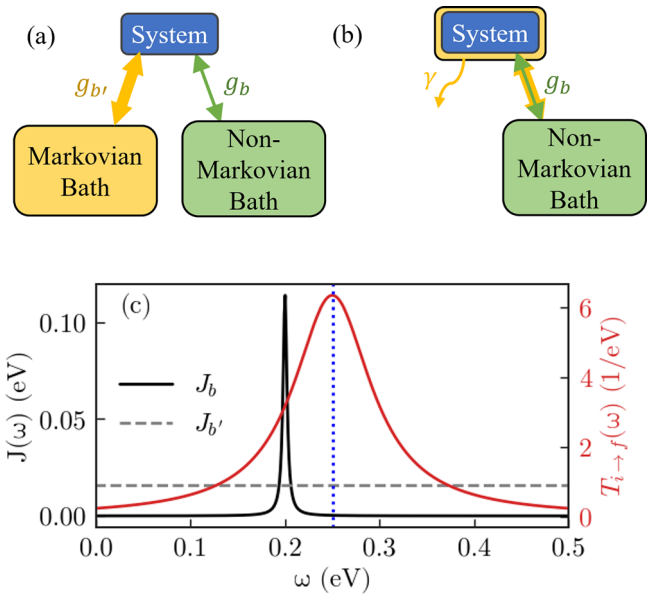

Fig. 1 | System coupled to Markovian and non-Markovian baths. a, **b** Two equivalent descriptions of a lossy system coupled to a non-Markovian bath with strength g_b. In **a**, losses are modeled through coupling $g_{b'}$ to a Markovian bath, while in (**b**) they are represented explicitly by the decay rate γ. In the latter case, the loss is an intrinsic property of the system, highlighted by the yellow background, and consequently the coupling to the non-Markovian bath (green arrow) is dressed by the interaction with the Markovian bath (yellow arrow). **c** Spectral densities of a non-Markovian bath (in black) and a Markovian bath (in grey) and an example of a transition spectrum between two lossy states ($T_{i\to f}(\omega)$ in red).

nonadditivity. We then benchmark BR LS against numerically exact simulations, demonstrating its higher accuracy compared to the standard Bloch-Redfield (BR) equation and confirming the effective memoryless behavior it assigns to the non-Markovian bath. Next, we quantify non-Markovianity using the trace distance method, showing that increasing system losses enhances the Markovian character of the dynamics and clarifying the distinct physical origin of this effect. Finally, we show that a transition-dependent effective spectral density for the non-Markovian bath emerges naturally within the BR LS framework, providing further insight into how the Markovian bath influences the non-Markovian one and suggesting a way to incorporate this influence within the standard BR formalism.

The BR LS approach: a memoryless master equation capturing baths' nonadditivity

We consider a quantum system coupled to two independent bosonic baths, one non-Markovian and the other Markovian, with the coupling strengths g_b and $g_{b'}$ as shown in Fig. 1a. This setup is described by the Hamiltonian:

$$\hat{H}_{s+b+b'} = \hat{H}_s + \hat{H}_b + \hat{H}_{b'} + g_b \hat{V}_s \hat{U}_b + g_{b'} \hat{V}'_s \hat{U}_{b'}, \tag{1}$$

where $\hat{H}_s, \hat{H}_b, \hat{H}_{b'}$ are the system and the two baths Hamiltonians; $\hat{V}_s, \hat{V}'_s$ are the system operators that couple to each bath and obey either $[\hat{V}_s, \hat{V}'_s] \neq 0$ or $[\hat{H}_s, \hat{V}'_s] \neq 0$[7]; and $\hat{U}_b = \int_0^\infty d\omega \sqrt{J_b(\omega)/g_b^2}(b_\omega + b_\omega^\dagger)$ and $\hat{U}_{b'} = \int_0^\infty d\omega \sqrt{J_{b'}(\omega)/g_{b'}^2}(b'_\omega + b'^\dagger_\omega)$ are the bath operators which couple them to the system, where b_ω, b'_ω ($b_\omega^\dagger, b'^\dagger_\omega$) are the bosonic annihilation (creation) operators of the baths, and $J_b(\omega)$, $J_{b'}(\omega)$ are their spectral densities, related to their autocorrelation functions (at zero temperature) by $C_b(t) = \int_0^\infty d\omega J_b(\omega) e^{-i\omega t}$ and $C_{b'}(t) = \int_0^\infty d\omega J_{b'}(\omega) e^{-i\omega t}$. We treat the situation where $J_b(\omega)$ is structured and sharp in energy, while $J_{b'}(\omega)$ is unstructured and even constant, as is exemplified in Fig. 1c. The width of the system-bath arrows in Fig. 1a, b indicates the Markovian (non-Markovian) character of the interaction, representing the associated broad (sharp) energy spectrum.

First, we use the memoryless character of the Markovian bath b', whose $C_{b'}(t)$ decays on a timescale much shorter than both the system dynamics and the interaction with the non-Markovian bath. The clear separation of timescales justifies treating the Markovian bath's influence locally on the system using a Lindblad master equation with operators acting directly on the system degrees of freedom[1,22]. This results in the master equation ($\hbar = 1$ here and later)

$$\begin{aligned}\frac{d\rho_{s+b}}{dt} &= -i[\hat{H}_s + \hat{H}_b + g_b \hat{V}_s \hat{U}_b, \rho_{s+b}] + \sum_{A'} \gamma_{A'} \hat{L}_{\hat{A}'}[\rho_{s+b}] \\ &= -i(\hat{\mathcal{H}}\rho_{s+b} - \rho_{s+b}\hat{\mathcal{H}}^\dagger) + \sum_{A'} \gamma_{A'} \hat{A}' \rho_{s+b} \hat{A}'^\dagger\end{aligned} \tag{2}$$

associated with the setup of a lossy system interacting with a non-Markovian bath presented in Fig. 1b using the total loss rate γ. Here, ρ_{s+b} is the density matrix that includes the degrees of freedom of the system and the non-Markovian bath. The system's interaction with the Markovian bath is encoded by the Lindblad superoperators: $\hat{L}_{\hat{A}'}[\rho] = \hat{A}'\rho\hat{A}'^\dagger - \frac{1}{2}\{\hat{A}'^\dagger\hat{A}', \rho\}$, where $\hat{A}'$ are the jump operators associated with the loss rates $\gamma_{A'}$ and originating from $\hat{V}'_s$ and $J_{b'}(\omega)$[1]. In the second line, we have rewritten the equation in terms of the effective non-Hermitian Hamiltonian $\hat{\mathcal{H}} = \hat{\mathcal{H}}_s + \hat{H}_b + g_b \hat{V}_s \hat{U}_b$, with $\hat{\mathcal{H}}_s = \hat{H}_s - \frac{i}{2}\sum_{A'} \gamma_{A'} \hat{A}'^\dagger \hat{A}'$[13], which describes the coherent part of the dynamics, including the dissipation to the Markovian bath due to the anticommutator in $\hat{L}_{\hat{A}'}[\rho]$. The remaining term describes the incoherent reappearance of this population after the dissipation-induced "quantum jumps". The NH character of $\hat{\mathcal{H}}_s$ implies that the system's energy levels acquire a finite linewidth. In the following, we demonstrate that this broadening plays a key role in accounting for the effect of the memoryless bath when evaluating the system's interaction with the non-Markovian one.

To treat the non-Markovian bath, we draw inspiration from BR theory[23,24], originally designed for the perturbative and Markovian regime of system-bath interactions and yielding the Lindblad description under a secular approximation[1]. We extend this framework by replacing the Hermitian Hamiltonian $\hat{H}_s$ with the non-Hermitian Hamiltonian $\hat{\mathcal{H}}_s$, which more accurately captures the system dynamics under the influence of the Markovian bath. This substitution effectively incorporates the influence of the Lindblad superoperators through the finite coherence lifetime and energy-level broadening encoded in $\hat{\mathcal{H}}_s$. As a result, these features enter naturally into the interaction with the non-Markovian bath and, as we will see below, allow the extended framework to capture the Markovianity of dynamics that would otherwise appear non-Markovian in standard BR theory. To achieve this, we describe the system density matrix $\rho_s(t)$ using the eigenstates of $\hat{\mathcal{H}}_s$ and its Hermitian conjugate $\hat{\mathcal{H}}_s^\dagger$. These eigenstates, denoted as $|i)$ for $\hat{\mathcal{H}}_s$ and $|j^*)$ for $\hat{\mathcal{H}}_s^\dagger$, where the notation $|\ldots)$, $(\ldots|$ rather than $|\ldots\rangle$, $\langle\ldots|$ is used to describe the right and left eigenstates of NH Hamiltonians[25], are associated with the complex eigenvalues $\omega_i - i\frac{\Gamma_i}{2}$ and $\omega_j + i\frac{\Gamma_j}{2}$, respectively. The real part $\omega_{i/j}$ encodes the states' energy, while the imaginary part $\Gamma_{i/j}$ encodes their loss rate, also associated with their linewidths[25]. The Markovian assumption is then applied while accounting for the decay of the states' norm and coherence by working in a frame that captures both these losses and the dynamics arising from the interaction with the non-Markovian bath. Consequently, this extended BR for lossy systems (BR LS) yields a memoryless master equation for $\rho_s(t)$ from the interaction between the lossy system (incorporating the influence of the Markovian bath) and the non-Markovian bath. The full derivation of the BR LS approach is given in Supplementary Note 1, and its benchmarking is discussed below.

The resulting BR LS master equation, including the effects of both baths, reads as

$$\frac{\mathrm{d}\rho_s(t)}{\mathrm{d}t} = -\,\mathrm{i}\,[\hat{H}_s, \rho_s(t)] + \sum_{A'} \gamma_{A'} \hat{L}_{\hat{A}'}[\rho_s] + \sum_{a,b,c,d} R_{abcd} |a)(c|\rho_s(t)|d^*)(b^*|, \tag{3}$$

where the Lindblad superoperators are also present in order to accurately describe the Markovian bath effect. The first term describes the system's internal dynamics, the second term encodes the dissipation induced by the memoryless bath, and the third term presents the influence of the non-Markovian bath dressed by the former dissipation and given by the BR LS tensor,

$$R_{abcd} = \delta_{bd} \sum_q F_{cdq} \tilde{V}_{aq} \tilde{V}_{qc} + \delta_{ac} \sum_q F^*_{dcq} \tilde{V}^*_{dq} \tilde{V}^*_{qb} - (F_{cda} + F^*_{dcb}) \tilde{V}_{ac} \tilde{V}^*_{db}, \tag{4}$$

where $\tilde{V}_{ij} = (i|\hat{V}_s|j)$, $\tilde{V}^*_{ij} = (i^*|\hat{V}_s|j^*)$, and $F_{jsq} = \int_0^\infty d\tau C_b(\tau) \mathrm{e}^{-\frac{1}{2}(\Gamma_q+\Gamma_s)\tau} \mathrm{e}^{-\mathrm{i}(\omega_q-\omega_j)\tau}$ is the one-sided Fourier transform of $C_b(t)$ evaluated at the complex frequency $\tilde{\omega}_{jsq} = \omega_j - \omega_q + \mathrm{i}\,\frac{\Gamma_s+\Gamma_q}{2}$. Importantly, Eq. (4) has the same computational complexity as the standard BR under a secular approximation, substituting complex frequency $\tilde{\omega}_{jjq}$ rather than a real one $\omega_j - \omega_q$, and it reproduces the standard BR tensor when neglecting the losses Γ_q, Γ_s[1,26]. In addition, similar to BR, it preserves the trace of the density matrix (see Supplementary Note 4). While the BR approach is accurate when $C_b(\tau)$ decays rapidly, as it happens for Markovian baths, BR LS only requires the rapid decay of $C_b(\tau)\mathrm{e}^{-\frac{1}{2}(\Gamma_q+\Gamma_s)\tau}$. Yet, BR LS captures different features from those obtained when retaining the full time dependence of the integral limits $\int_0^t$ in the BR tensor. While such a time-dependent BR approach would capture the imperfect frequency resolution over short time scales, BR LS instead takes into account the system's finite linewidths and nonadditive effects. Thus, it sheds light on the interplay between the two baths in inducing memoryless dynamics, showing that when the Markovian bath causes sufficiently fast loss of coherence in the system, the influence of a nominally non-Markovian bath can be described by a Markovian term using R_{abcd}.

The BRLS approach introduced above is relevant for any system featuring losses and weakly interacting with an external bath, independently from the Markovian bath responsible for its losses. It obtains accurate results also when the quantum jump terms associated with the Markovian bath are relevant for the dynamics, as happens, e.g., when they describe dephasing instead of decay (see Supplementary Note 7). However, BR LS is not valid when the losses are larger than the system's energies and the Lindblad formalism may introduce artificial pumping of the ground state[27]. Moreover, similar to BR[28], it can violate positivity when the weak-coupling assumption for the interaction with the non-Markovian bath breaks down.

BR LS performance in reproducing the numerically exact dynamics

We apply the BRLS for a cavity-quantum electrodynamical (QED) setup in which quantum emitters are strongly coupled to a cavity light mode. These setups, which attract great attention and offer the manipulation of quantum properties of both light and matter[29–34], can often be described in terms of two different baths. The first, electromagnetic, one induces decay of the cavity mode due to absorption and radiation losses, as well as spontaneous emission of the emitters. It often has a broad spectrum and is therefore Markovian[14]. The second bath describes phonon-exciton interactions and can be highly structured and therefore non-Markovian. Specifically, several types of emitters used in cavity QED setups, such as molecular J- and H-aggregates[35–37] or quantum dots[38,39], can be described as two-level emitters coupled to structured phononic baths. Then, the effective NH system Hamiltonian for an ensemble of N emitters, including the coherent parts of the Lindblad operators $\gamma_c \hat{L}_{\hat{A}'=a}$ and $\gamma_e \hat{L}_{\hat{A}'=\sigma^j_-}$, is given by the NH Tavis-Cummings (TC) model[40]:

$$\hat{\mathcal{H}}_s = \tilde{\omega}_c a^\dagger a + \sum_j^N \left[\tilde{\omega}_e \sigma^j_+ \sigma^j_- + \frac{g_{ec}}{\sqrt{N}} (a^\dagger \sigma^j_- + \sigma^j_+ a) \right]. \tag{5}$$

Here, a ($a^\dagger$) and σ^j_- (σ^j_+) are the annihilation (creation) operators for the cavity mode and the j-th emitter, respectively, and the coupling strength between the cavity mode and each emitter is $g_{ec}/\sqrt{N}$. The energies in Eq. (5) are complex due to the coupling to the Markovian bath, denoted by $\tilde{\omega}_c = \omega_c - \frac{i}{2}\gamma_c$ and $\tilde{\omega}_e = \omega_e - \frac{i}{2}\gamma_e$, where the loss of the cavity mode γ_c can be very large, particularly for metallic nanocavities or nanoresonators, which can achieve the strong-coupling regime in the emitter-cavity interaction[41–45]. Furthermore, each emitter is coupled to a different non-Markovian phononic bath through the coupling operator $\hat{V}^j_s = \sigma^j_+ \sigma^j_-$.

In the following, we study the population transfer between the eigenstates of $\hat{\mathcal{H}}_s$ given in Eq. (5), which vanishes in the absence of the phononic baths (i.e., for $g_b = 0$ and $J_b(\omega) = 0$), thereby isolating the dynamics they induce (see Supplementary Fig. S1 and Supplementary Note 3). This isolation relies on the decay-only structure of the Markovian bath in this example; however, the BR LS approach remains applicable even when the Markovian bath induces dephasing (see Supplementary Note 7). When $g_{ec} > \frac{|\gamma_c - \gamma_e|}{4}$ and $\omega_e = \omega_c$, $\hat{\mathcal{H}}_s$ has two hybrid light-matter eigenstates, known as polaritons, with complex energies $\omega_e \pm g_{ec} - \frac{i}{2}\Gamma_p$ where $\Gamma_p = \frac{\gamma_e+\gamma_c}{2}$ is their loss rate. The lower-energy state is typically called the lower polariton (LP), while the higher-energy state is known as the upper polariton (UP). The other states arising when $N \geq 2$ are pure excitonic states with the complex energy $\tilde{\omega}_e$, usually termed as dark states (DS)[46].

As a test case, we consider a single emitter ($N = 1$ in Eq. (5)) with an, in principle, non-Markovian phononic bath whose spectral density is plotted in black in Fig. 1c and given by

$$J_b(\omega) = \Theta(\omega) \frac{2g_b^2}{\pi} \frac{\kappa\omega\omega_b}{(\omega^2 - \omega_b^2)^2 + \kappa^2\omega^2}, \tag{6}$$

where $\Theta(\omega)$ is the Heaviside function that is zero for $\omega < 0$, $\omega_b = 0.2$ eV, $\kappa = 5$ meV and $g_b = 0.03$ eV. No thermal population of the bath is considered. This test case can be solved by the numerically exact discretization method (detailed in the supplemental material of ref. 27), which directly discretizes the bath and treats the complete lossy system coupled to non-Markovian bath setup. We use it to benchmark BR LS and analyze the Markovian character of the dynamics. In Fig. 2, we compare the population of the LP calculated by the BR LS and the numerically exact approaches as a function of the Rabi splitting $\omega_{\mathrm{UP}} - \omega_{\mathrm{LP}} \approx 2g_{ec}$ and the time t, where the initial state is the UP, $\gamma_c = 0.1$ eV, $\gamma_e = 0.1$ meV and $\omega_c = \omega_e$. In addition, we present in Fig. 2c the population transfer obtained by the standard BR method that treats the phononic bath independently from the system losses[46]. The absolute differences between BR LS and BR and the exact results are presented in Supplementary Fig. S3. As BR is incapable of treating non-Markovian baths and does not account for the interplay between the two baths, the results that it yields (Fig. 2c) significantly differ from the exact results (Fig. 2a). However, the BR LS (Fig. 2b) obtains much better agreement, particularly for times longer than the lifetime of the states, i.e., $t > \tau_p = \frac{1}{\Gamma_p} \approx 13$ fs, verifying the memory loss of the interaction with the non-Markovian bath due to the system loss as assumed within the BR LS. In Supplementary Fig. S4, we show that similar agreement is obtained for all elements of the system density matrix, not just the populations. Furthermore, we show in Supplementary Fig. S5 that BR LS also provides good agreement with the exact results when the Markovian bath induces pure dephasing instead of decay, i.e., is described by a Lindblad superoperator given by $\gamma_c \hat{L}_{A'=a^\dagger a}$. These checks confirm the generality of BR LS.

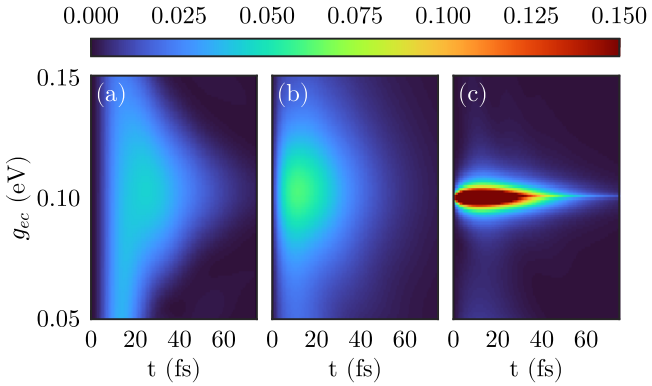

Fig. 2 | Bath-driven population transfer obtained by different approaches. The population of the lower polariton (LP) of Eq. (5) ($N = 1$) obtained by **a** the numerically exact calculation, **b** the introduced Bloch-Redfield for lossy systems (BR LS), and **c** the standard Bloch-Redfield (BR), when only the upper polariton (UP) is populated at $t = 0$. g_{ec} represents half the energy difference between the UP and LP. The spectral density of the phononic bath driving the population transfer is plotted in black in Fig. 1(c).

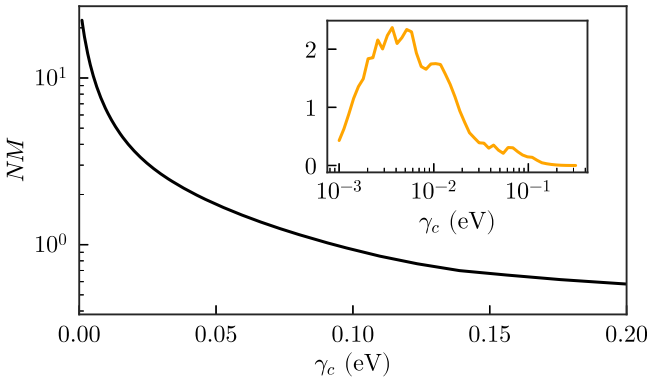

Fig. 3 | Non-Markovianity measured by the trace distance method. The solid black line presents the non-Markovianity (NM) during the whole time evolution, while the orange one, plotted in the inset, takes into account just the dynamics occurring after the system's lifetime $\frac{2}{\gamma_c} \approx \tau_p$.

Measuring the non-Markovianity as a function of the system losses using the trace distance method

To highlight that the introduction of losses into the system increases the Markovianity of its dynamics, which can then be described by the memoryless BR LS approach, we use the trace distance method[47], designed for measuring the non-Markovianity in open quantum systems, to analyze the test case studied in Fig. 2. In this approach, the non-Markovianity is computed by

$$NM = \sum_j [D(\rho_1^m(t_{f,j}), \rho_2^m(t_{f,j})) - D(\rho_1^m(t_{i,j}), \rho_2^m(t_{i,j}))]. \quad (7)$$

Here, $D(\rho_1^m(t), \rho_2^m(t))$ is the trace distance between two density matrices of the system, $\rho_1^m(t), \rho_2^m(t)$, associated with different initial states and yielding the maximal sum in Eq. (7), where the index j sums over all the time intervals $(t_{i,j}, t_{f,j})$ for which the trace distance increases. We treat the non-Markovian bath using the numerically exact discretization method, and similar to ref. 47, identify the optimal pair of $\rho_1^m(t), \rho_2^m(t)$ by sampling 500^2 pairs of initial states of the form $(C_c a^\dagger + \sqrt{1 - C_c^2} e^{i\phi} \sigma_+)|0\rangle$, where the coefficient C_c varies from 0 to 1 and the phase ϕ from 0 to 2π. This yields the optimal pair: $\rho_1^m(0) = |+\rangle\langle+|, \rho_2^m(0) = |-\rangle\langle-|$, where $|\pm\rangle = \frac{1}{\sqrt{2}}(\sigma_+ \pm i a^\dagger)|0\rangle$. In Fig. 3, we plot the computed non-Markovianity, describing the backflow of information from the non-Markovian bath into the system, as a function of γ_c, where $g_{ec} = 0.1$ eV (such that the UP-LP transition is resonant with the peak of the phononic spectral density) and the other parameters are the same as for Fig. 2. As can be seen, the non-Markovianity drops when the system loss, reflecting the coupling with the Markovian bath, increases. This confirms the transfer of Markovianity between the baths.

In addition, to emphasize the distinct mechanism for Markovianity, which arises from the short lifetime of the system rather than from the rapid decay of the bath autocorrelation function, we plot in the inset of Fig. 3 the value of NM calculated by Eq. (7), but restricted to time intervals $(t_{i,j}, t_{f,j})$ satisfying $t_{i,j} > 2/\gamma_c \approx \tau_p$. While at low loss, this quantity increases with γ_c (due to the inclusion of more intervals), the trend reverses for $\gamma_c > \kappa = 5$ meV, i.e., when the system decays faster than the bath's autocorrelation function. In this regime, the Markovianity of the dynamics is governed not by the bath's memory time but by the system's inability to retain coherence long enough to resolve temporal features of the bath autocorrelation function. As a result, the non-Markovianity approaches zero, indicating that the dynamics become effectively Markovian for times longer than the system lifetime, even though the bath itself is non-Markovian. This observation aligns with the agreement between BR LS and the exact results shown in Fig. 2.

Transition-dependent effective spectral density for the non-Markovian bath

The numerically exact results shown in Fig. 2a present bath-driven population transfer over a larger range of Rabi splittings than would be expected from inspecting the bandwidth of the bath spectral density $J_b(\omega)$ presented in Fig. 1c. We use the BR LS approach to show that this broadening stems from the broad linewidth of the energy-dependent transition spectrum, given by $T_{i\to f}(\omega) = \frac{1}{\pi} \frac{\frac{1}{2}(\Gamma_i + \Gamma_f)}{(\omega_i - \omega_f - \omega)^2 + \frac{1}{4}(\Gamma_i + \Gamma_f)^2}$ for each transition between two lossy states $i \to f$, and exemplified in red in Fig. 1c for $\Gamma_i = \Gamma_f = \Gamma_p$ and $\omega_i - \omega_f = 0.25$ eV. The standard BR approach misses this effect (Fig. 2c), evaluating the transfer rate $K_{UP\to LP}$ only through the spectral density at the energy difference between the states associated with the maximum of $T_{\mathrm{UP}\to\mathrm{LP}}(\omega)$ (e.g., at the vertical dashed blue line in Fig. 1(c)). Then, $K^{BR}_{\mathrm{UP}\to\mathrm{LP}} = 2\pi J_b(2g_{ec})|\tilde{V}_{\mathrm{UP}\to\mathrm{LP}}|^2$[46] where $\tilde{V}_{\mathrm{UP}\to\mathrm{LP}} = (\mathrm{LP}|\hat{V}_s|\mathrm{UP})$. In contrast, BR LS captures the broadening of the states (Fig. 2b), and for each transition $i \to f$ naturally yields an effective spectral density that can be written as

$$J^{\mathrm{eff}}_{i\to f}(\omega_i - \omega_f) = \int_0^\infty d\omega J_b(\omega) T_{i\to f}(\omega), \quad (8)$$

such that $K^{\mathrm{BR\,LS}}_{\mathrm{UP}\to\mathrm{LP}} = 2\pi J^{\mathrm{eff}}_{\mathrm{UP}\to\mathrm{LP}}(2g_{ec})|\tilde{V}_{\mathrm{UP}\to\mathrm{LP}}|^2$ (see Supplementary Note 2). $J^{\mathrm{eff}}_{\mathrm{UP}\to\mathrm{LP}}(2g_{ec})$ is a convolution of $J_b(\omega)$ with $T_{\mathrm{UP}\to\mathrm{LP}}(\omega)$, highlighting the role of the system in mediating the transfer of Markovianity between the two baths. We emphasize that Eq. (8) describes effective spectral densities for the system's interaction with the non-Markovian bath, which are different for each system transition $i \to f$, in contrast to the case of hierarchical environments[48–50] where the baths directly interact with each other, and their combined effect can be described by a single spectral density including solely their properties.

Finally, we analyze whether the BR LS can be reproduced with the standard BR by replacing the spectral density $J_b(\omega)$ with a suitably broadened effective density as given by Eq. (8). To do so, we consider the structured spectral density $J_0(\omega)$, plotted in black in Fig. 4, which has been taken from ref. 51 and scaled down by two orders of magnitude to ensure weak coupling between nuclear and electronic degrees of freedom, as appropriate for J-aggregates[35]. Moreover, we consider $N = 30$ emitters in the system described by Eq. (5), such that the system has dark states in addition to upper and lower polaritons. The other parameters are the same as for the test case above. Three transitions can occur in this setup: UP → LP, UP → DS, and DS → LP. Since $T_{\mathrm{UP}\to\mathrm{DS}} = T_{\mathrm{DS}\to\mathrm{LP}}$, the last two transitions correspond to the same effective spectral density, $J_1^{\mathrm{eff}}(\omega)$, plotted in orange in Fig. 4. However, the transition UP → LP that features a broader $T_{\mathrm{UP}\to\mathrm{LP}}$ corresponds to another and broader effective spectral density, $J_2^{\mathrm{eff}}(\omega)$, plotted in light blue in Fig. 4. As can be seen, both $J_1^{\mathrm{eff}}(\omega)$ and $J_2^{\mathrm{eff}}(\omega)$ are

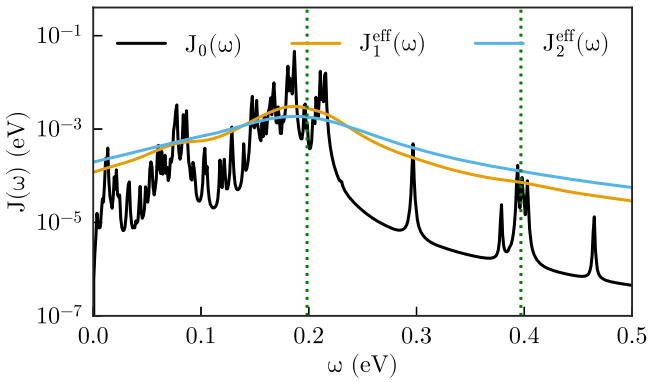

Fig. 4 | Structured and effective smooth spectral densities. The original spectral density $J_0(\omega)$ models the vibrational structure of a J-aggregated dye (black), while the effective spectral densities, defined in Eq. (8), correspond to the transitions from the upper polariton (UP) to dark states (DS) and from the DS to the lower polariton (LP) ($J_1^{\text{eff}}(\omega)$), and from the UP to the LP ($J_2^{\text{eff}}(\omega)$). The dotted green lines indicate the energies of these transitions when $g_{ec} = 0.2$ eV.

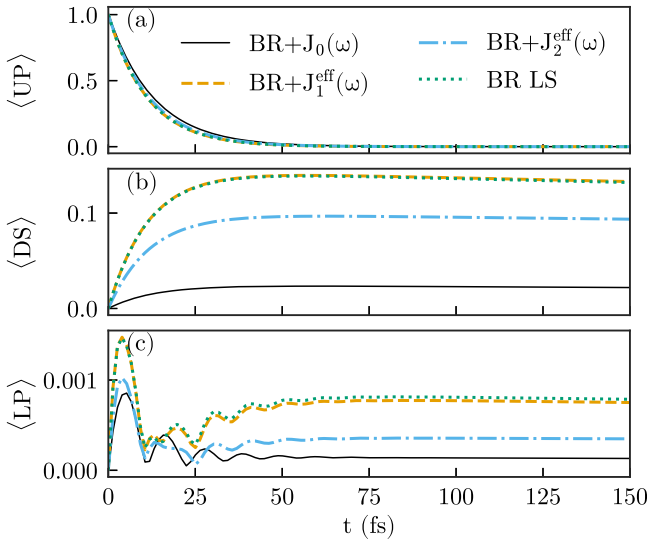

Fig. 5 | Analyzing the use of effective spectral densities. Populations of **a** the upper polariton (UP), **b** dark states (DS), and **c** the lower polariton (LP) are shown as a function of time, obtained using the standard Bloch-Redfield (BR) with the original and effective spectral densities, and using the Bloch-Redfield for lossy systems (BR LS) approach. Here, 30 two-level emitters, interacting with the vibrational bath shown in black in Fig. 4, are strongly coupled to a lossy cavity ($g_{ec} = 0.2$ eV).

much smoother than $J_0(\omega)$, again indicating that a non-Markovian bath can become Markovian when acting on a lossy system.

Figure 5 presents the population of the UP, DS and LP obtained by BR using $J_0(\omega)$, $J_1^{\text{eff}}(\omega)$ and $J_2^{\text{eff}}(\omega)$ and by BR LS for $g_{ec} = 0.2$ eV, when the UP is initially populated. Due to the complexity of the system, its exact solution is untractable. The vertical lines in Fig. 4 present the energy differences between the states, i.e., $\omega_{\text{UP}} - \omega_{\text{DS}} = \omega_{\text{DS}} - \omega_{\text{LP}} \approx g_{ec}$ and $\omega_{\text{UP}} - \omega_{\text{LP}} \approx 2g_{ec}$. Since the spectral densities are larger for the UP → DS transition than for the UP → LP one, and due to the presence of many dark states, the dynamics in Fig. 5 is dominated by the UP → DS transition, followed by the DS → LP transition. Therefore, the results obtained by BR+ $J_1^{\text{eff}}(\omega)$, associated with these transitions, are in excellent agreement with the BR LS results. This confirms that we can extract a linewidth-dependent effective spectral density from the BR LS approach to describe the system's interaction with the non-Markovian bath. However, the results obtained by BR+ $J_2^{\text{eff}}(\omega)$ as well as by BR + $J_0(\omega)$, which underestimates the spectral density at $\omega = g_{ec}$, present a smaller population transfer to the dark states and therefore to the lower polariton as well. Note that the slight difference in the population of the lower polariton between BR LS and BR+ $J_1^{\text{eff}}(\omega)$ originates from the contribution of the UP → LP transition, underestimated by $J_1^{\text{eff}}(\omega)$ since $J_1^{\text{eff}}(2g_{ec}) < J_2^{\text{eff}}(2g_{ec})$. Moreover, the oscillations appearing in Fig. 5c are caused by the bath-induced Lamb shift of the system's energy levels[52].

Conclusions

We have demonstrated that the interaction between a system and two independent baths, one Markovian and one non-Markovian, can result in memoryless dynamics, driven by the interplay between the baths. Furthermore, the interaction with the non-Markovian bath itself becomes memoryless, as dissipation induced by the system's interaction with the Markovian bath modifies its influence. To capture this phenomenon, we introduced the BR LS approach, extending traditional Bloch-Redfield theory to account for Markovian dynamics due to system losses rather than bath properties. By effectively averaging over the non-Markovian bath's spectral density, our approach can be viewed as a coarse-graining of system-bath interactions[53] that emerges naturally from intrinsic system dissipation. This method provides an efficient way to compute the dynamics of lossy systems weakly coupled to a non-Markovian bath, particularly in regimes where standard approaches fail and more computationally intensive methods[54–56] are typically required. Given the prevalence of lossy systems in various fields, including optics[14], acoustics[15], quantum thermodynamics[16–18], and chemistry[19–21], our findings enhance both the understanding of system-bath interactions and the computational efficiency of modeling complex systems, opening up new possibilities for studying open quantum systems in these domains.

Data availability

The authors declare that the data supporting the findings of this study are available within the manuscript and its Supplementary Information file. The numerical source data for Figs. 2-5 are given in Supplementary Data 1.

Code availability

The numerical results presented in this work were obtained using QuTiP 4.7[57]. Functions implementing BR LS are available from the authors upon reasonable request.

Received: 14 March 2025; Accepted: 4 September 2025;
Published online: 10 October 2025

References

1. Breuer, H.-P. & Petruccione, F. The theory of open quantum systems. *Oxford University Press, USA* (2002).
2. de Vega, I. & Alonso, D. Dynamics of non-Markovian open quantum systems. *Rev. Mod. Phys.* **89**, 015001 (2017).
3. Dhahri, A. & Mukhamedov, F. Open quantum random walks, quantum Markov chains and recurrence. *Rev. Math. Phys.* **31**, 1950020 (2019).
4. Noé, F. & Rosta, E. Markov models of molecular kinetics. *J. Chem. Phys*. **151**, 190401 (2019).
5. Vicentini, F., Biella, A., Regnault, N. & Ciuti, C. Variational neural-network ansatz for steady states in open quantum systems. *Phys. Rev. Lett.* **122**, 250503 (2019).
6. Ghoshal, A. & Sen, U. Multiparty Spohn's theorem for a combination of local Markovian and non-Markovian quantum dynamics. *Phys. Rev. A* **110**, 012451 (2024).
7. Kołodyński, J., Brask, J. B., Perarnau-Llobet, M. & Bylicka, B. Adding dynamical generators in quantum master equations. *Phys. Rev. A* **97**, 062124 (2018).
8. Chan, C.-K., Lin, G.-D., Yelin, S. F. & Lukin, M. D. Quantum interference between independent reservoirs in open quantum systems. *Phys. Rev. A* **89**, 042117 (2014).
9. Gribben, D. et al. Exact dynamics of nonadditive environments in non-Markovian open quantum systems. *PRX Quantum* **3**, 010321 (2022).

10. Maguire, H., Iles-Smith, J. & Nazir, A. Environmental nonadditivity and Franck-Condon physics in nonequilibrium quantum systems. *Phys. Rev. Lett.* **123**, 093601 (2019).
11. McConnell, C. & Nazir, A. Electron counting statistics for non-additive environments. *J. Chem. Phys*. **151**, 054104 (2019).
12. Bundgaard-Nielsen, M., Mørk, J. & Denning, E. V. Non-Markovian perturbation theories for phonon effects in strong-coupling cavity quantum electrodynamics. *Phys. Rev. B* **103**, 235309 (2021).
13. Roccati, F., Palma, G. M., Ciccarello, F. & Bagarello, F. Non-Hermitian physics and master equations. *Open Syst. Inf. Dyn.* **29**, 2250004 (2022).
14. Medina, I., García-Vidal, F. J., Fernández-Domínguez, A. I. & Feist, J. Few-mode field quantization of arbitrary electromagnetic spectral densities. *Phys. Rev. Lett.* **126**, 093601 (2021).
15. Kitzman, J. et al. Phononic bath engineering of a superconducting qubit. *Nat. Commun.* **14**, 3910 (2023).
16. Brandner, K., Bauer, M. & Seifert, U. Universal coherence-induced power losses of quantum heat engines in linear response. *Phys. Rev. Lett.* **119**, 170602 (2017).
17. Tajima, H. & Funo, K. Superconducting-like heat current: Effective cancellation of current-dissipation trade-off by quantum coherence. *Phys. Rev. Lett.* **127**, 190604 (2021).
18. Zhang, J.-W. et al. Dynamical control of quantum heat engines using exceptional points. *Nat. Commun.* **13**, 6225 (2022).
19. Landau, A., Bhattacharya, D., Haritan, I., Ben-Asher, A. & Moiseyev, N. Ab initio complex potential energy surfaces from standard quantum chemistry packages. *Adv. Quantum Chem.* **74**, 321 (2017).
20. Gelbwaser-Klimovsky, D., Aspuru-Guzik, A., Thoss, M. & Peskin, U. High-voltage-assisted mechanical stabilization of single-molecule junctions. *Nano Lett.* **18**, 4727 (2018).
21. Jech, M. et al. Quantum chemistry treatment of silicon-hydrogen bond rupture by nonequilibrium carriers in semiconductor devices. *Phys. Rev. Appl.* **16**, 014026 (2021).
22. Lindblad, G. On the generators of quantum dynamical semigroups. *Commun. Math. Phys.* **48**, 119 (1976).
23. Wangsness, R. K. & Bloch, F. The dynamical theory of nuclear induction. *Phys. Rev.* **89**, 728 (1953).
24. Redfield, A. G. Nuclear magnetic resonance saturation and rotary saturation in solids. *Phys. Rev.* **98**, 1787 (1955).
25. Moiseyev, N. *Non-Hermitian quantum mechanics*. (Cambridge University Press, 2011).
26. Peskin, U. *Quantum Mechanics in Nanoscience and Engineering*. (Cambridge University Press, 2023).
27. Lednev, M., García-Vidal, F. J. & Feist, J. Lindblad master equation capable of describing hybrid quantum systems in the ultrastrong coupling regime. *Phys. Rev. Lett.* **132**, 106902 (2024).
28. Hartmann, R. & Strunz, W. T. Accuracy assessment of perturbative master equations: Embracing nonpositivity. *Phys. Rev. A* **101**, 012103 (2020).
29. Galego, J., Garcia-Vidal, F. J. & Feist, J. Suppressing photochemical reactions with quantized light fields. *Nat. Commun.* **7**, 13841 (2016).
30. Zhong, X. et al. Energy transfer between spatially separated entangled molecules. *Angew. Chem.* **129**, 9162 (2017).
31. Garcia-Vidal, F. J., Ciuti, C. & Ebbesen, T. W. Manipulating matter by strong coupling to vacuum fields. *Science* **373**, eabd0336 (2021).
32. Raimond, J.-M., Brune, M. & Haroche, S. Manipulating quantum entanglement with atoms and photons in a cavity. *Rev. Mod. Phys.* **73**, 565 (2001).
33. Reiserer, A. & Rempe, G. Cavity-based quantum networks with single atoms and optical photons. *Rev. Mod. Phys.* **87**, 1379 (2015).
34. Wang, D. et al. Turning a molecule into a coherent two-level quantum system. *Nat. Phys.* **15**, 483 (2019).
35. Spano, F. Optical microcavities enhance the exciton coherence length and eliminate vibronic coupling in j-aggregates. *J. Chem. Phys*. **142**, 184707 (2015).
36. Herrera, F. & Spano, F. C. Cavity-controlled chemistry in molecular ensembles. *Phys. Rev. Lett.* **116**, 238301 (2016).
37. Sáez-Blázquez, R., Feist, J., Fernández-Domínguez, A. I. & García-Vidal, F. Organic polaritons enable local vibrations to drive long-range energy transfer. *Phys. Rev. B* **97**, 241407 (2018).
38. Grange, T. et al. Reducing phonon-induced decoherence in solid-state single-photon sources with cavity quantum electrodynamics. *Phys. Rev. Lett.* **118**, 253602 (2017).
39. Peng, K. & Rabani, E. Polaritonic bottleneck in colloidal quantum dots. *Nano Lett.* **23**, 3452–3459 (2023).
40. Tavis, M. & Cummings, F. W. Exact solution for an n-molecule—radiation-field hamiltonian. *Phys. Rev.* **170**, 379 (1968).
41. Törmä, P. & Barnes, W. L. Strong coupling between surface plasmon polaritons and emitters: a review. *Rep. Prog. Phys.* **78**, 013901 (2014).
42. Chikkaraddy, R. et al. Single-molecule strong coupling at room temperature in plasmonic nanocavities. *Nature* **535**, 127 (2016).
43. Zhang, Y. et al. Sub-nanometre control of the coherent interaction between a single molecule and a plasmonic nanocavity. *Nat. Commun.* **8**, 15225 (2017).
44. Kongsuwan, N. et al. Suppressed quenching and strong-coupling of purcell-enhanced single-molecule emission in plasmonic nanocavities. *ACS Photonics* **5**, 186 (2018).
45. Baumberg, J. J. et al. Extreme nanophotonics from ultrathin metallic gaps. *Nat. Mater.* **18**, 668 (2019).
46. del Pino, J., Feist, J. & Garcia-Vidal, F. J. Quantum theory of collective strong coupling of molecular vibrations with a microcavity mode. *N. J. Phys.* **17**, 053040 (2015).
47. Breuer, H.-P., Laine, E.-M. & Piilo, J. Measure for the degree of non-Markovian behavior of quantum processes in open systems. *Phys. Rev. Lett.* **103**, 210401 (2009).
48. Ma, T., Chen, Y., Chen, T., Hedemann, S. R. & Yu, T. Crossover between non-Markovian and Markovian dynamics induced by a hierarchical environment. *Phys. Rev. A* **90**, 042108 (2014).
49. Fruchtman, A., Lovett, B. W., Benjamin, S. C. & Gauger, E. M. Quantum dynamics in a tiered non-Markovian environment. *N. J. Phys.* **17**, 023063 (2015).
50. Man, Z.-X., An, N. B. & Xia, Y.-J. Non-Markovian dynamics of a two-level system in the presence of hierarchical environments. *Opt. Express* **23**, 5763 (2015).
51. Zhao, D. et al. Impact of vibrational modes in the plasmonic Purcell effect of organic molecules. *ACS Photonics* **7**, 3369 (2020).
52. Lamb, W. E. Jr & Retherford, R. C. Fine structure of the hydrogen atom by a microwave method. *Phys. Rev.* **72**, 241 (1947).
53. Lorenzoni, N. et al. Systematic coarse graining of environments for the nonperturbative simulation of open quantum systems. *Phys. Rev. Lett.* **132**, 100403 (2024).
54. del Pino, J., Schröder, F. A., Chin, A. W., Feist, J. & Garcia-Vidal, F. J. Tensor network simulation of non-Markovian dynamics in organic polaritonics. *Phys. Rev. B* **98**, 165416 (2018).
55. Prior, J., Chin, A. W., Huelga, S. F. & Plenio, M. B. Efficient simulation of strong system-environment interactions. *Phys. Rev. Lett.* **105**, 050404 (2010).
56. Strathearn, A., Kirton, P., Kilda, D., Keeling, J. & Lovett, B. W. Efficient non-Markovian quantum dynamics using time-evolving matrix product operators. *Nat. Commun.* **9**, 3322 (2018).
57. Johansson, J. R., Nation, P. D. & Nori, F. QuTiP: An open-source Python framework for the dynamics of open quantum systems. *Comput. Phys. Commun.* **183**, 1760 (2012).

Acknowledgements

This work has been funded by the Spanish Ministry of Science, Innovation and Universities-Agencia Estatal de Investigación through grants PID2021-126964OB-i00, PID2021-125894NB-i00, EUR2023-143478, and CEX2018-000805-M (through the María de Maeztu program for Units of Excellence in R&D). We also acknowledge financial support from the European Union's

Horizon Europe Research and Innovation Program through agreement 101070700 (MIRAQLS). In addition, this project received funding from the European Union's Horizon 2020 research and innovation program under the Marie Skłodowska-Curie Grant Agreement No 101034324.

Author contributions

A.B.-A., A.I.F.D and J.F developed the idea and discussed the results. A.B.-A. performed the numerical calculations and wrote the first draft of the manuscript, which was revised and edited by all authors.

Competing interests

The authors declare no competing interests.

Additional information

Supplementary information The online version contains supplementary material available at https://doi.org/10.1038/s42005-025-02310-y.

Correspondence and requests for materials should be addressed to Anael Ben-Asher, Antonio I. Fernández-Domínguez or Johannes Feist.

Peer review information *Communications Physics* thanks Paul Menczel and the other anonymous reviewer(s) for their contribution to the peer review of this work.